Assessment of the Validity of the Double Superhelix Model for Reconstituted High Density Lipoproteins
A COMBINED COMPUTATIONAL-EXPERIMENTAL APPROACH*[S]

Martin K. Jones[‡§], **Lei Zhang**[¶‖], **Andrea Catte**[‡§], **Ling Li**[‡], **Michael N. Oda**[**], **Gang Ren**[¶‖], **and Jere P. Segrest**[‡§1]

From the [‡]Department of Medicine and Atherosclerosis Research Unit, [§]Center for Computational and Structural Dynamics, University of Alabama, Birmingham, Alabama 35294, the [¶]Molecular Foundry, Lawrence Berkeley National Laboratory, Berkeley, California 94720, the [‖]Department of Biochemistry and Biophysics, University of California, San Francisco, California 94158, and the [**]Children's Hospital Oakland Research Institute, Oakland, California 94609-1673

For several decades, the standard model for high density lipoprotein (HDL) particles reconstituted from apolipoprotein A-I (apoA-I) and phospholipid (apoA-I/HDL) has been a discoidal particle ~100 Å in diameter and the thickness of a phospholipid bilayer. Recently, Wu *et al.* (Wu, Z., Gogonea, V., Lee, X., Wagner, M. A., Li, X. M., Huang, Y., Undurti, A., May, R. P., Haertlein, M., Moulin, M., Gutsche, I., Zaccai, G., Didonato, J. A., and Hazen, S. L. (2009) *J. Biol. Chem.* 284, 36605–36619) used small angle neutron scattering to develop a new model they termed double superhelix (DSH) apoA-I that is dramatically different from the standard model. Their model possesses an open helical shape that wraps around a prolate ellipsoidal type I hexagonal lyotropic liquid crystalline phase. Here, we used three independent approaches, molecular dynamics, EM tomography, and fluorescence resonance energy transfer spectroscopy (FRET) to assess the validity of the DSH model. (i) By using molecular dynamics, two different approaches, all-atom simulated annealing and coarse-grained simulation, show that initial ellipsoidal DSH particles rapidly collapse to discoidal bilayer structures. These results suggest that, compatible with current knowledge of lipid phase diagrams, apoA-I cannot stabilize hexagonal I phase particles of phospholipid. (ii) By using EM, two different approaches, negative stain and cryo-EM tomography, show that reconstituted apoA-I/HDL particles are discoidal in shape. (iii) By using FRET, reconstituted apoA-I/HDL particles show a 28–34-Å intermolecular separation between terminal domain residues 40 and 240, a distance that is incompatible with the dimensions of the DSH model. Therefore, we suggest that, although novel, the DSH model is energetically unfavorable and not likely to be correct. Rather, we conclude that all evidence supports the likelihood that reconstituted apoA-I/HDL particles, in general, are discoidal in shape.

High density lipoproteins (HDL) represent a heterogeneous population of particles with apoA-I as the major protein (1). Whether apoA-I/HDL[2] plays a direct role in cardiovascular disease prevention (*e.g.* removal of cholesterol from clogged arteries) or an indirect one (*e.g.* acts as a platform for the clustering of protective molecules, such as anti-inflammatory or antioxidant proteins), detailed knowledge of HDL structure is a key to understanding the molecular mechanism underlying these processes. Because the conformation of apoA-I on HDL is highly plastic (1), understanding apoA-I/HDL structure and dynamics is not straightforward.

Since the early 1970s, the standard model for HDL particles reconstituted from apolipoprotein A-I (apoA-I) and phospholipid (apoA-I/HDL) has been that of a discoidal particle on the order of 100 Å in diameter and the thickness of a phospholipid bilayer. The initial observation of discoidal HDL particles was made by Forte *et al.* (2) when they examined HDL from patients with familial lecithin:cholesterol acyltransferase deficiency by negative stain EM. Reconstituted apoA-I/HDL particles (3) and nascent HDL from lymph (4) were then observed by negative stain EM to also have a discoidal shape. X-ray and neutron scattering studies (5, 6) provided further support for the standard discoidal model.

The standard discoidal model has been used to interpret the results of a large number of experimental studies of the structure of reconstituted apoA-I/HDL particles. For review, see Refs. 7–10.

Recently, however, Wu *et al.* (11) used small angle neutron scattering to develop a model for apoA-I/HDL particles that is dramatically different from the standard model. In their model, termed a double superhelix (DSH), apoA-I possesses an open helical shape that twists around a central prolate ellipsoidal particle resembling a partial type I hexagonal lyotropic liquid crystalline phase.

The DSH model is interesting. It is similar to MD simulation-based models (12) in that the proposed double superhelix forms a left-handed spiral as it wraps around the prolate ellip-

[2] The abbreviations used are: apoA-I/HDL, reconstituted HDL; CGMD, coarse-grained molecular dynamics; DSH, double superhelix; MD, molecular dynamics; MDSA, molecular dynamics simulated annealing; POPC, palmitoyloleoylphosphatidylcholine; VMD, visual molecular dynamics; r.m.s.d., root mean square deviation; UC, unesterified cholesterol; AE-DANS, N-(iodoacetyl)-N'-(1-sulfo-5-naphthyl)ethylenediamine; NS, negative stain; SANS, small angle neutron scattering; CG, coarse-grained.

soid-shaped lipid micelle. The major difference between the protein conformations of the models is that in the DSH model the terminal domains are separated at opposite ends of the ellipsoidal structure, although in MD models the terminal domains wrap back to self-associate (12). Despite several reservations we have, the small angle neutron diffraction results published by Wu *et al.* (11) to support the DSH model are not trivial. Given the innumerable structural studies of reconstituted apoA-I/HDL particles that have incorporated the standard discoidal model as their central paradigm, it seemed imperative to us to assess the validity of the DSH model.

We decided upon a combined computational-experimental approach of MD simulations, EM tomography, and fluorescence resonance energy transfer (FRET) spectroscopy. By using two quite different MD methods, all-atom simulated annealing (MDSA) (12, 13) and coarse-grained simulation (CGMD) (13, 14), we found that the initial ellipsoidal DSH particle rapidly collapsed with either method to form essentially identical discoidal structures. Examination of apoA-I/HDL particles having comparable compositions to the DSH model by two independent tomography approaches, negative stain (NS) EM and electron cryo-microscopy (cryo-EM), revealed the presence of three-dimensional discoidal structures. Finally, using FRET, reconstituted apoA-I/HDL particles show a 28–34-Å intermolecular separation between terminal domain residues 40 and 240, a separation that is incompatible with the DSH model; the expected distance is 125 Å. Based upon these results, we conclude that, although interesting and novel, the DSH model is energetically unfavorable and not likely to be correct.

EXPERIMENTAL PROCEDURES

Computational Studies

Creation and Simulation of Particles—The all-atom model of the DSH particle (initial structure) was obtained from the Protein Model Data base (accession no. PM0075984). The cavity throughout the central long axis of the prolate ellipsoidal lipid structure and the packing defects between the acyl chains (see Fig. 8*A*) were removed by deletion of water molecules placed there by Visual Molecular Dynamics (VMD) (15) solvation to create empty space, followed by MD simulation of the subsequent solvated particle at 310 K and 1 bar for 5 ns. This simulation resulted in rapid collapse of the empty space between acyl chains by 2 ns; although the space has collapsed, considerable disorder in the packing of the terminal methyl groups occurs (see Fig. 8*B*) because of the problem of packing terminal methyls in cylindrical micelles like the hexagonal I phase lipid. This particle (starting structure) was then subjected twice in succession to the following MDSA protocol (all at 1 bar) (12, 13): heated from 310 to 500 K in 20 ps, simulated at 500 K for 10 ns, cooled from 500 to 420 K in 2 ns, cooled from 420 to 400 K in 5 ns, cooled from 400 to 310 K in 3 ns, and finally simulated at 310 K for 10 ns, giving a total duration of 30 ns per MDSA and thus 65 ns total.

A discoidal apoA-I/HDL all-atom particle made with the palmitoyloleoylphosphatidylcholine (POPC):unesterified cholesterol (UC):apoA-I stoichiometry of the DSH model, 200:

20:2, was created from an initial 252(POPC):2(apoA-I) particle; this allows full-length apoA-I to entirely encircle the particle and is the way we have dealt with the N-terminal portion of apoA-I for which no good structural model exists (12, 13). From this particle, 32 POPC were deleted and 20 POPC were mutated to UC to give us a particle with the same stoichiometry as the Hazen models. Then the resultant particle was simulated at 310 K and 1 bar for 5 ns and subjected once to the MDSA protocol.

All-atom simulations were performed using NAMD (16) as described in Catte *et al.* (17). Each system was solvated with the solvation plug-in of VMD (15) (the solvent was extended to at least 20 Å on each side) and then ionized and charge-neutralized with NaCl to 0.15 M with the autoionize plug-in. The TIP3P water model was used (18). The CHARMM22 (19, 20) and -27 (21, 22) force fields were used for protein and lipid molecules, respectively.

The DSH particle (after the first 310 K 5-ns simulation, the "starting structure") was course-grained with the VMD "CG Builder" plug-in. Secondary structure assignments for the apoA-I protein were set for the course-grained (CG) simulation from these coordinates using the program DSSP (23), except that all Pro residues were set to turn, the first two N- and C-terminal residues were set to coil and the Gly-Gly-Ala (residues 185–187) were set to turn. This particle was simulated for an effective time of 65.6 μs.

CGMD simulations were performed on the starting structure using GROMACS 4.0 (24) and the MARTINI force-field 2.1 (20, 25) as described in Catte *et al.* (14). Each system was solvated with CG water (the solvent was extended to at least 20 Å on each side) and ionized and charge-neutralized to 0.15 M with CG Na$^+$ and Cl$^-$ ions.

The partial atom model (without hydrogens) of the DSH particle that was simulated for 60 ns by Hazen and co-workers (26) was obtained from the Hazen data web page of Lerner Research Institute, Department of Cell Biology, Cleveland Clinic. This model was converted to an all-atom model using psfgen within VMD. The resulting particle was solvated and ionized as above, and then solvent and ions were removed from the central cavity. This system was simulated at 310 K for 10 ns.

Root Mean Square Deviation Calculations—The root mean square deviations (r.m.s.d.) of protein α-carbon atoms were calculated for the DSH and 200:20:2 all-atom particles over the entire lengths of the 60-ns double MDSA and 30-ns MDSA trajectories, respectively. Each r.m.s.d. was calculated with respect to the particle coordinates after the initial 310 K 5-ns simulation (starting structure). For the CG simulation, the r.m.s.d. of protein α-carbon beads was calculated over the entire length of the 65.6-μs effective time trajectory, with respect to the beginning coordinates.

Experimental Studies

Reconstituted ApoA-I/HDL Sample Preparation—The apoA-I/HDL samples for electron cryo-tomography data collection were provided by the laboratory of Dr. Jianjun Wang (27) at Wayne State University, Detroit, MI, and the apoA-I/HDL samples for NS electron tomography data collection

were provided by the laboratory Dr. Michael Oda (28) at Children's Hospital Oakland Research Institute, Oakland, CA.

Preparation of NS Specimens—We previously proposed an optimized NS protocol (29) in which a 2.5-μl drop of apoA-I/HDL solution was placed on a thin carbon-coated 300 mesh copper grid (Cu-300CN, Pacific Grid-Tech, San Francisco) that had been glow-discharged. After ~1 min, excess solution was blotted with filter paper by touching from the edge. The grid was washed by touching it briefly to the surface of a drop (~30 μl) of distilled water at ~4 °C, and then excess solution were removed by touching with filter paper. This was repeated three times. Three drops (~30 μl) of uranyl formate negative stain were then applied successively; excess stain was removed in the same fashion as the water drops, except the last drop. The grid was exposed to the last drop of stain for 1–3 min in the dark before excess solution was removed, and grid was dried in air at room temperature.

Preparation of Cryo-EM Specimens—Cryo-EM specimens were prepared as described previously (30) with modifications. In brief, apoA-I/HDL was diluted to 0.2 mg/ml with Dulbecco's PBS (DPBS: 2.7 mM KCl, 1.46 mM KH$_2$PO$_4$, 136.9 mM NaCl, and 8.1 mM Na$_2$HPO$_4$; Invitrogen), and a 3-μl aliquot was adhered to a glow-discharged holey carbon film coated copper 300 mesh grid (Cu-300HN, Pacific Grid-Tech, San Francisco, CA) for 1 min. Instead of blot-drying, the samples were blotted with filter paper from both sides for 2 s at 100% humidity and 4 °C with a FEI Vitrobot rapid-plunging device and then flash-frozen in liquid ethane. The flash-frozen grids were transferred into liquid nitrogen for storage.

Electron Tomography Data Collection—NS and cryo-EM specimens were examined with an FEI Tecnai T12 transmission electron microscope (Philips Electron Optics/FEI) operating at 120 kV. While using the microscope for vitrified samples, the micrographs were acquired with a high sensitivity 4,096 × 4,096-pixel Gatan UltraScan CCD camera at ×67,000 magnification and −180 °C conditions. Each pixel of the micrograph corresponds to 1.73 Å in the specimens. The apoA-I/HDL specimens were mounted on a Gatan 626 high tilt cryo-sample holder. The tilt series of specimens and tomography data set were controlled and imaged by UCSF tomography software that was preinstalled in the microscope (31). The tilt angle ranged from −69 to 69° in steps of 1.5°, and the total illumination electron dose was ~140 e$^-$/Å^2. For NS specimens, the microscope was operated under the same conditions but with a high tilt tomography room temperature holder and with a total dose of ~200 e$^-$/Å^2 or more.

Fluorescent ApoA-I Preparation—A Trp-deficient variation of apoA-I (W@∅) was produced by substituting the four endogenous Trp residues (positions 8, 50, 72, and 108) with phenylalanine. A single Trp-bearing apoA-I, W@40, was created by substituting tryptophan for lysine at position 40 in W@∅ to generate W@40 apoA-I. A single cysteine substitution was introduced at position 240 in W@40 apoA-I to yield W@40:L240C. The W@∅ and W@40 apoA-I variants have been employed in previous FRET experiments and have yielded consistent results (28, 32, 33). N-(Iodoacetyl)-N'-(1-sulfo-5-naphthyl)ethylenediamine (AEDANS) labeling of W@40:L240C was performed as described previously (8). Briefly, 8

mg of W@40:L240C was reduced by incubating for 8 h at room temperature in the presence of tris(2-carboxyethyl)-phosphine at a final molar ratio of W@40:L240C to tris(2-carboxyethyl)phosphine = 1:10. The reduced protein was immobilized on a nickel-chelating column (1 ml of Hi-Trap Chelating HP columns, GE Healthcare) and pre-washed with 40 mM imidazole and 3 M guanidine in phosphate-buffered saline, pH 7.4. A 10-fold molar excess of AEDANS (Molecular Probes, Inc.), with respect to apoA-I concentration, was passaged onto the apoA-I-loaded Hi-Trap chelating column in 3 M guanidine HCl and incubated for 3 h at 37 °C. Labeled protein was eluted by 0.5 M imidazole and dialyzed extensively against TBS (8.2 mM Tris, 150 mM NaCl, 1 mM EDTA, pH 7.4) to remove guanidine HCl and unreacted label. Labeling of cysteine substitution variants of apoA-I with AEDANS has yielded an apoA-I with lipid binding properties analogous to WT apoA-I (8, 28).

Preparation of Fluorescently Labeled Reconstituted ApoA-I/HDL Particles—Reconstituted nascent HDL were prepared by a modified method originally described by Nichols *et al.* (34, 35). 22 mM sodium deoxycholate (in 0.5 ml) was added to an equal volume of 16.3 mM POPC in Tris-buffered saline, pH 8. The mixture was vortexed and incubated at 37 °C until clear. The solution was added (1:2 (w/w) apoA-I to POPC) to 3 mg of apoA-I (W@∅, W@40 to W@∅ (1:5 ratio), and W@40:L240C to W@∅ (1:5 ratio)), followed by incubation at 37 °C for 1 h. Sodium deoxycholate was removed by extensive dialysis against Tris-buffered saline, pH 7.4. Reconstituted apoA-I/HDL particles were recovered by KBr density gradient ultracentrifugation at 50,000 × g for 3 h in a Beckman Optima TLA 100.4 rotor. Fractions containing both protein and lipid were pooled and dialyzed against Tris-buffered saline, pH 7.4. Reconstituted HDL particles were separated on a Superdex 200 preparation grade XK 16/100 column (GE Healthcare), run at a flow rate of 1.5 ml/min in TBS, pH 8.0. The 9.6-nm fraction was collected and concentrated using Vivaspin-6 10,000 molecular weight cutoff ultrafiltration devices (Sartorius Biotech Inc.). The size of reconstituted apoA-I/HDL particles was confirmed by native gradient gel electrophoresis (34).

Fluorescence Spectroscopy—Fluorescence measurements were conducted by excitation of samples containing reconstituted apoA-I/HDL particles at 295 nm, and emission spectra were monitored between 300 and 575 nm on a HORIBA Jobin Yvon FluoroMax-4 spectrofluorometer (HORIBA Scientific). Scans were performed on 0.5 mg/ml protein with a 3-nm slit width and scan rate of 30 nm/min. The distance between specified donor (Trp) and acceptor (AEDANS) fluorophores was calculated as described by Selvin (36).

RESULTS

Computational Studies—Fig. 1 shows cross-eyed stereo images of the starting all-atom and coarse-grained DSH models viewed from opposite sides. Fig. 1, *A* and *B*, shows all-atom images of the full model and the protein alone, respectively. Fig. 1, *C* and *D*, shows cross-eyed images of the stereo coarse-grained full model and protein alone, respectively. Note the wide separation (77 Å) of the two N termini (*white*) and C
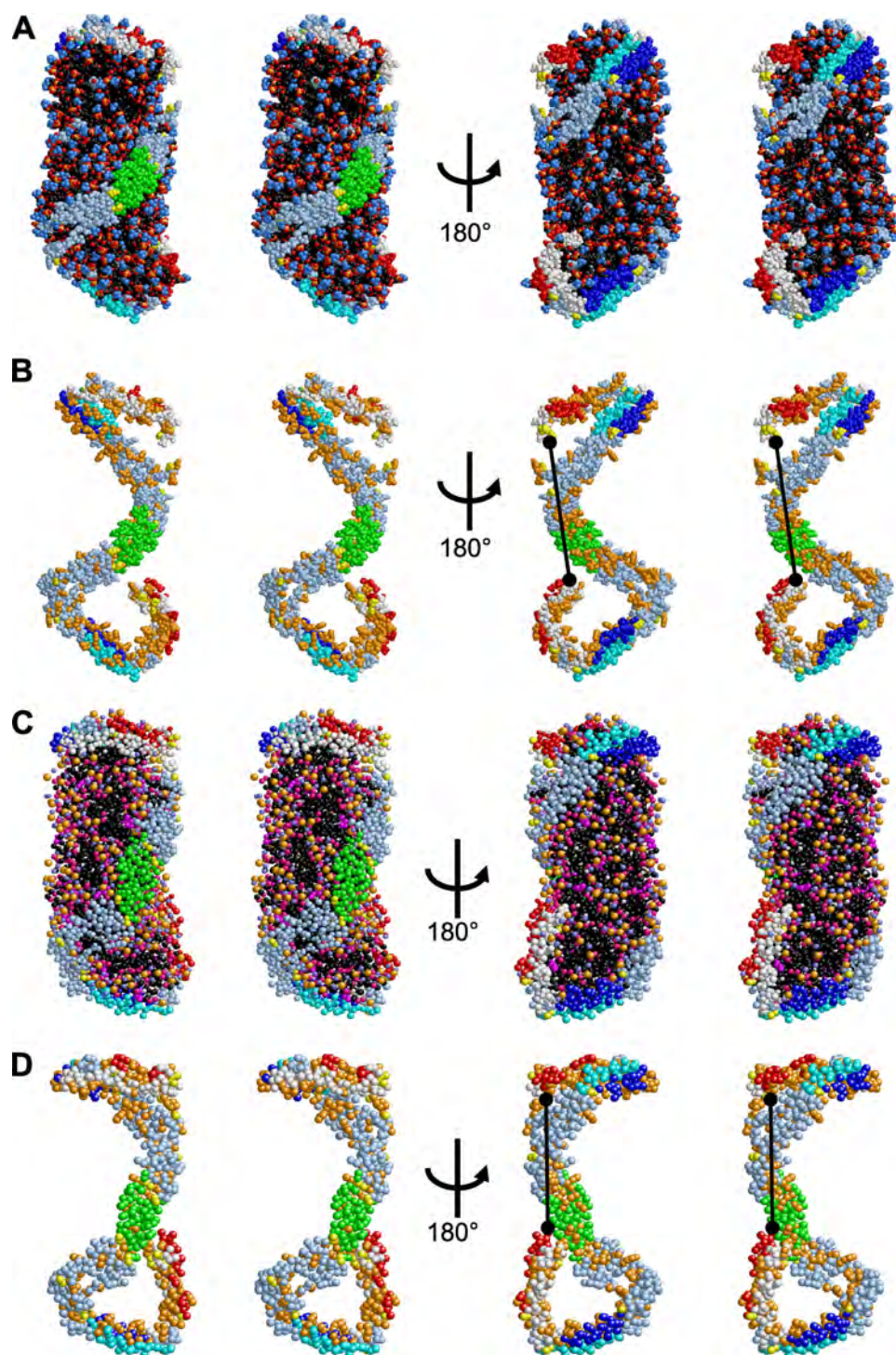
FIGURE 1. **Cross-eyed stereo images of the starting all-atom and coarse-grained DSH model made with Rasmol.** *Color code* used is as follows. Protein: G* domain (residues 1–43), *white*; helix 5, *green*; helix 8, *cyan*; helix 10, *red*; the remainder of protein is *slate blue*; prolines, *yellow*. POPC: acyl chains, *black*; P, *gold*; cholines, *sky blue*. UC, *magenta*. The *left-hand* images are rotated 180° to create the *right-hand* images. *A,* starting DSH model for nascent HDL used in MDSA simulations. *B,* protein alone; the distance between the N and C termini is indicated by the *black bar. C,* starting DSH model in *A* that was coarse-grained and used in CGMD simulations. *D,* protein alone; the distance between the N and C termini is indicated by the *black bar.*

termini (*red*) domain pairs (*black lines* in Fig. 1, *B* and *D*, *right-hand* images).

Fig. 2*A* is a r.m.s.d. plot of the trajectories of the sequential all-atom MDSA simulations compared with the starting DSH model. The last 10 ns of MDSA-1 and the last 20 ns of MDSA-2 are flat, indicating equilibration. Fig. 2*B* is a r.m.s.d.

plot of the trajectories of the CGMD simulation compared with the starting coarse-grained DSH model. The plot reaches a maximum r.m.s.d. of ~30 Å by 350-ns equivalents (0.35 µs), declines slightly to 25 Å by 20 µs, and then is flat to 60 µs.

Fig. 3, *A* and *B*, shows space-filling models viewed from the lipid-rich side showing intermediates in the collapse of the
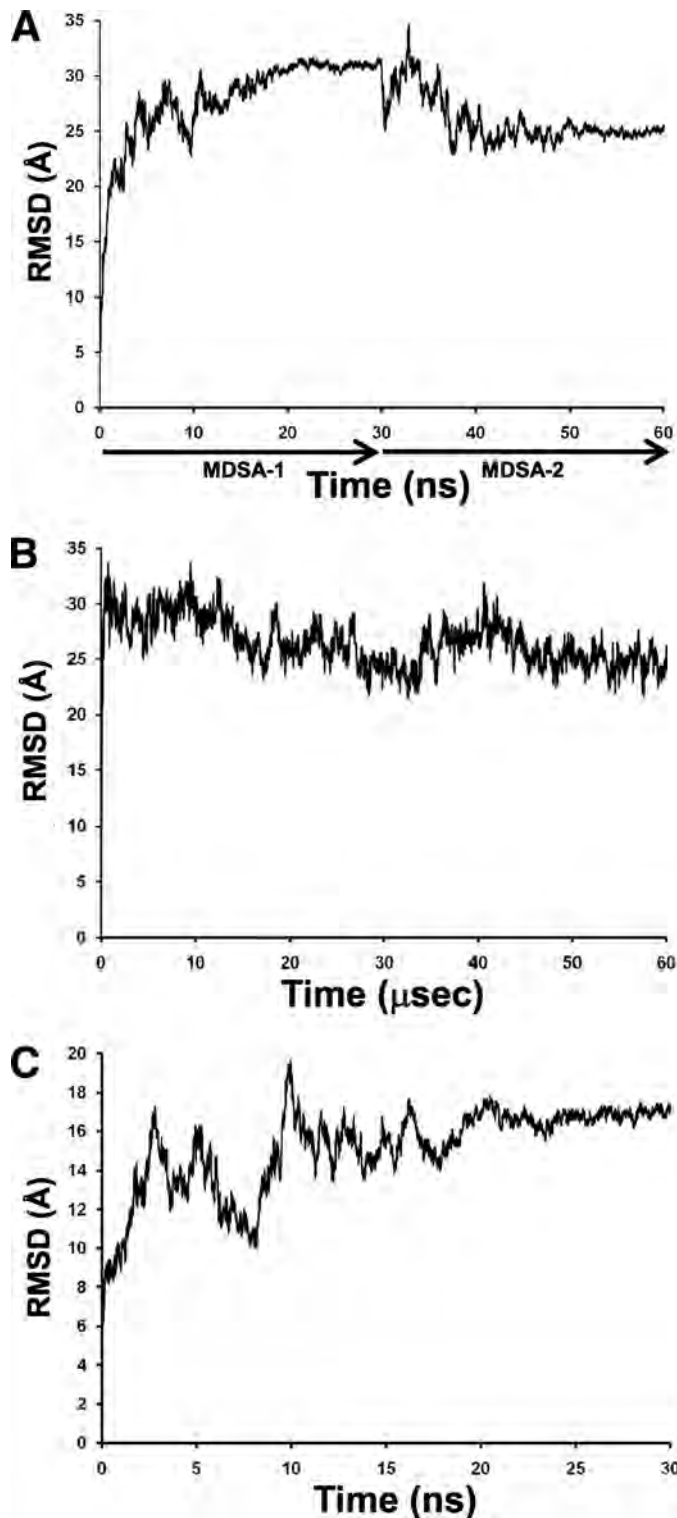
FIGURE 2. **r.m.s.d. plots for the three MD simulations.** *A,* r.m.s.d. *versus* time for the two consecutive MDSA simulations of the starting all-atom DSH model**.** *B,* r.m.s.d. *versus* time for the CGMD simulation of the starting CG DSH model. *C,* r.m.s.d. *versus* time for the MDSA simulation of the starting discoidal model containing 200 POPC, 20 UC, and 2 apoA-I.

starting DSH structure to a discoidal shape during MDSA and CGMD simulations, respectively. The starting structure in the MDSA simulation has begun to collapse by 2 ns and forms a discoidal or oblate ellipsoidal shape by 4 ns with an r.m.s.d. of

26.8 Å. The starting structure in the CGMD simulation forms a discoidal shape by 320 ns with an r.m.s.d. of 16.8 Å. The collapse from the prolate ellipsoidal to the oblate ellipsoidal disc shape begins on the lipid-rich side of both particles (Fig. 1, *A* and *C*, *right-hand panels*); this portion of the particle is essentially a hexagonal I phase lipid micelle unmodified by protein and therefore should be the most unstable arrangement of lipids in the DSH model.

Fig. 4, *A* and *B,* represents a series of cross-eyed stereo images of different views of the final structures after two sequential 30-ns MDSA simulations of the starting all-atom DSH model and a single 60-μs CGMD simulation of the coarse-grained DSH model, respectively. The most striking feature of these structures, generated by quite different MD methods, is their similarity. Although the termini of both structures are still widely separated (65 Å each), both structures form bilayers that are discoidal in shape (Fig. 4, *A* and *B*, *side* and *slab views*), have a large patch of acyl chains ~80 Å wide exposed to solvent along one edge of the bilayer disc (Fig. 4, *A* and *B*, *double-arrowed arcs, top views*), and have a J-shaped loop at one end of their double belt that creates the patch of exposed acyl chains (Fig. 4, *A* and *B, side views*). This patch of exposed acyl chains would be unstable and could not exist without something covering it, such as a portion of the apoA-I double belt (see Fig. 4*C*) or another apolipoprotein, such as apoA-II. This suggests strongly that the final structures in Fig. 4, *A* and *B,* are kinetically trapped; relaxation to complete disc coverage as in Fig. 4*C* would require impractically longer times of simulation.

Thus two features of the MD simulations suggest that the starting DSH model is intrinsically unstable.(i) The starting CG model subjected to MD simulation at 310 K rapidly collapses into a discoidal shape, achieving an r.m.s.d. of 17 Å by 320 ns and a maximum r.m.s.d. of 30 Å by 1.28 μs. (ii) The final shapes of the MDSA and CGMD simulations are discoidal, and the conformations of the protein components are very similar, and this is significant because these two methods of MD simulation possess different strengths and weaknesses (13).

Fig. 4*C* shows cross-eyed stereo images of different views of an all-atom MDSA simulation starting from a discoidal apoA-I/HDL particle made with the stoichiometry of the DSH model, 200:20:2. This panel shows that the N- and C-terminal domains at the end of the simulation cover the exposed patch of acyl chains seen in Fig. 4, *A* and *B.* The r.m.s.d. plot of this simulation in Fig. 2*C* shows that the particle has equilibrated after 30 ns of MDSA simulation.

Electron Tomographic Studies—Fig. 5 shows a series of tomographic images produced by stage tilting of negative stain EM (Fig. 5*A*) and cryo-EM (Fig. 5, *B–G*) preparations of reconstituted apoA-I/HDL particles with a stoichiometry of 160(POPC):8(UC):2(apoA-I). Although the contrast for the cryo-EM is less than that for the negative stain images, both EM tomographic methods clearly show that the reconstituted apoA-I/HDL particles are discoidal in shape in three dimensions. The cryo-EM tomographic images shown in Fig. 5*G* are especially informative regarding the structure of the near native state of particles embedded in vitreous ice. The particle
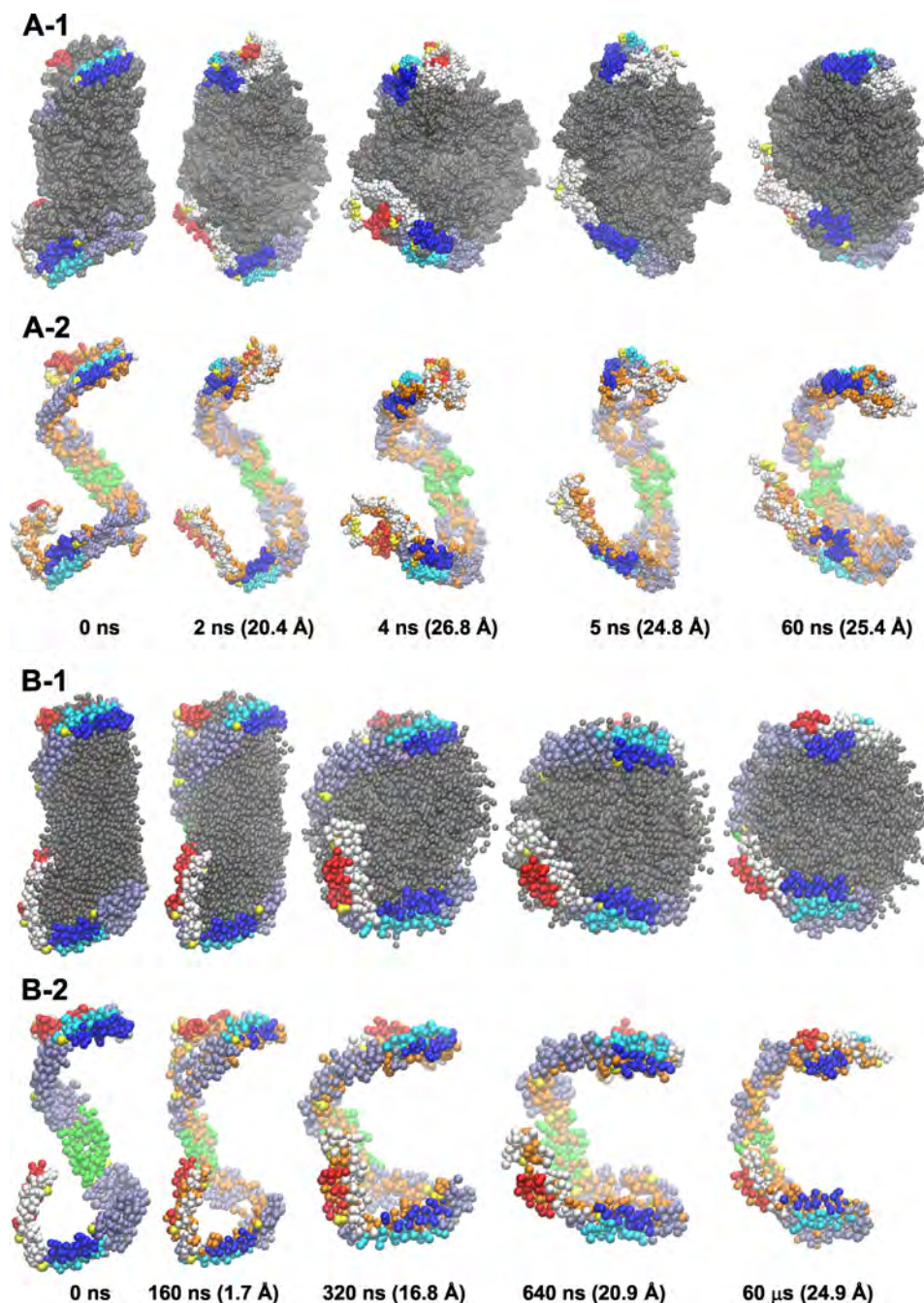
FIGURE 3. **Space-filling models made with VMD using depth-cueing viewed from the lipid-rich side showing intermediates in the collapse of the starting DSH structure to a discoidal shape during MDSA and CGMD simulations.** *Color code,* same as for Fig. 1. *A,* structure of MDSA simulation at 0, 2, 4, 5, and 60 ns. *A-1,* Entire particle. *A-2,* protein only. r.m.s.d. for protein in each structure is shown in *parentheses. B,* structure of CGMD simulation at 0, 0.16, 0.32, 0.64, and 60 μs equivalents. *B-1,* entire particle. *B-2,* protein only. r.m.s.d. for protein in each structure is shown in *parentheses.*

whose disc plane lies perpendicular to the axis of stage tilt (lower image) remains an edge-on disc following stage tilt, although the particle whose disc plane lies parallel to the axis of stage tilt (upper image) changes from an edge-on view to a face-on view of the disc after a stage tilt of 66°.

Energy Transfer Studies—In a FRET experiment, a Trp residue served as the energy donor (emission maximum 330 to 350 nm; excitation 295 nm), although the extrinsic fluorescence probe, AEDANS, covalently bound to an engineered Cys residue, served as the energy acceptor (emission maximum ~467 nm; excitation 336 nm). To limit the number of

potential fluorescence donors in apoA-I, for all the apoA-I used in this experiment intrinsic Trp residues (Trp-8, Trp-50, Trp-72, and Trp-108) were substituted for Phe, generating apoA-I(W@Ø). The energy donor (Trp) was positioned at residue 40 through a K40W substitution in apoA-I(W@Ø), yielding W@40 (see under "Experimental Procedures"). W@40 was AEDANS-labeled by introducing a cysteine substitution at residue 240 (L240C), yielding W@40:L240C-AE (see under "Experimental Procedures"). W@40:L240C-AE in a 1:5 ratio with W@Ø was used to create 9.6 nm diameter discoidal apoA-I/HDL for intramolecular distance measurements. This
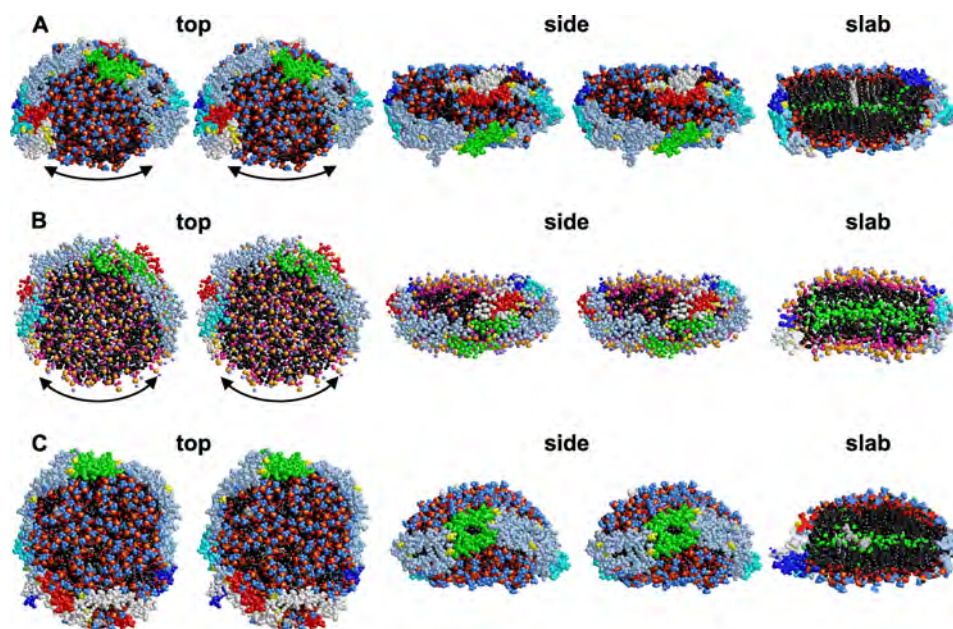
FIGURE 4. **Final structures of all-atom and coarse-grained MD simulations of the starting DSH model compared with an all-atom 30-ns MD simulation of a discoidal model containing 200 POPC, 20 UC, and 2 apoA-I.** All images were made with Rasmol. *Color code*, same as for Fig. 1. Each structure is shown from the top and side in cross-eyed stereo and as a nonstereo cross-sectional view of each structure from the side. *A,* MDSA of the starting all-atom model simulated for 60 ns. *B,* CGMD simulation of the starting coarse-grained DSH model simulated for 60 μs. *C,* all-atom 30-ns MD simulation of a discoidal model containing 200 POPC, 20 UC, and 2 apoA-I.

ratio of labeled protein to unlabeled ensures that ~83% of labeled protein is paired with an unlabeled protein, minimizing the contribution of inter-molecular FRET. The resulting rHDL elicited significant FRET ($E = 0.24$; average of three samples), as judged by the fluorescence emission intensity at 470 nm upon excitation of the sample at 295 nm (Fig. 6) and as measured from background corrected spectra comparing Trp fluorescence (integrated from 310 to 425 nm) W@40: L240C-AE to W@40. Based on the observed E values, we calculated $R \cong 28-34$ Å.

DISCUSSION

The low resolution nature of small angle neutron scattering (SANS) is a weakness in the original derivation of the DSH model (11). The essential first step in development of the DSH model was the fitting of SANS data collected from deuterated apoA-I nascent HDL to the following three models: (i) low resolution protein and lipid shapes of the DSH model, (ii) a double helical belt model, and (iii) the solar flare model that is essentially a double helical belt model containing symmetrical segments (residues 159–180) detached from the disc edge (37). The three models were fitted to the SANS scattering intensity for protein (contrast matched to protein to test the coil shape of the DSH protein) or the SANS scattering intensity for lipid (contrast matched to lipid to test the prolate ellipsoidal shape of the DSH lipid).

Relevant to model iii, Shih *et al.* (38) recently published both all-atom and coarse-grained MD simulations of the solar flare model (37). After their simulations, the protruding solar flare loops (residues 159–180) in both the original solar flare model and the corrected model collapsed, and the salt bridges proposed to stabilize the solar flares broke. The original models contained right docking interfaces that were stacked, thus

creating a clockwise N- to C-terminal rotation viewed from the top of the disc with hydrophobic residues facing the solvent, and the corrected model contained the correct LL ring pair orientation (left docking interfaces were stacked creating a counterclockwise N- to C-terminal rotation viewed from the top of the disc) with hydrophobic residues facing the lipid (39). Our published MD simulations of apoA-I/HDL particles show that the 159–180-residue region (helix 6-helix 7 junction) in the larger R2-2 particles forms a relatively stable helix, but with size shrinkage to the R2-1 and R2-0 particles, this region becomes less helical but never forms a protruding loop, although other regions, such as portions of helix 8, always form loops (12).

Relevant to model i, the weaker of the two curve fits is to the lipid shape. The double belt model fits the SANS data almost as well as the DSH model. Furthermore, the authors do not show lipid fit for the various MD-generated saddle-shaped models (minimal surface models) that are prolate ellipsoidal in shape in their own right (12, 17).

Although Hazen and co-workers (26) consider minimal surface or saddle-shaped variations of the double helical belt model, all of their models are essentially 100% helical. Because significant segments of the MD simulated models contain nonhelical regions that loop off the disc edge (12), and because the MD models are not symmetrical in protein conformation (12, 17), MD simulations, rather than 100% helical models, would have been better for SANS protein fitting.

A second weakness in the SANS data is that the ratio of 200 POPC to 2 apoA-I used does not form stable dimeric (R2) apoA-I particles (12, 40). Because SANS data collection takes many hours, particle fusion may have occurred during this long time in the neutron beam, thus confusing the curve fitting.
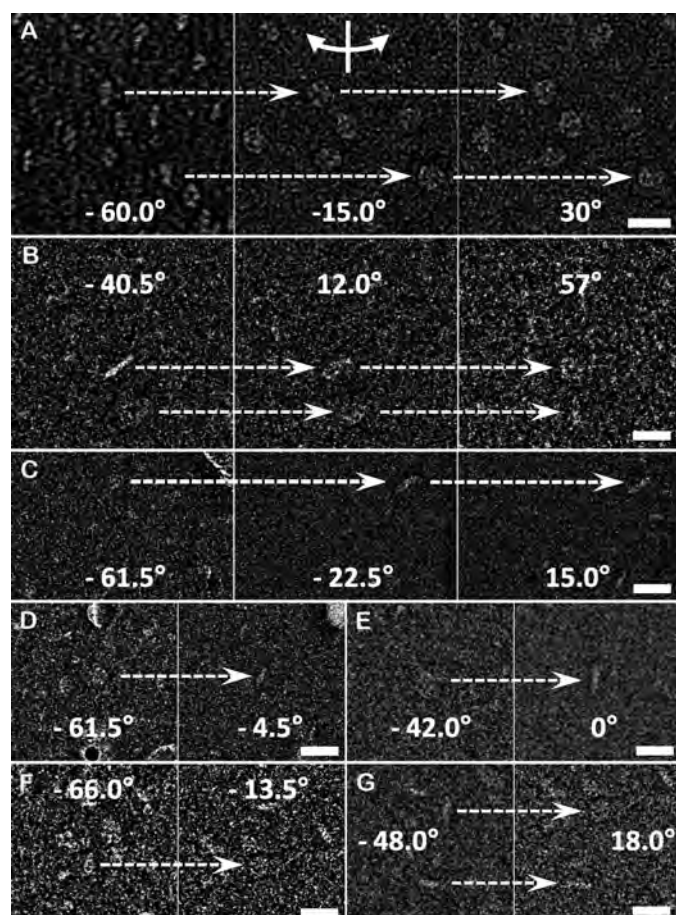
FIGURE 5. **Discoidal shapes of reconstituted apoA-I/HDL particles revealed by negative stain and electron cryo-tomography.** In each view the axis of tilt is vertical to the images (diagrammatically illustrated in *upper* and *bottom center* of *A*). Selected titled images are linked by *dotted arrows*. Relative tilt angles are indicated in each image. *Scale bars,* 200 Å. *A,* three selected tilted views of apoA-I/HDL particles from one negative stain electron microscopic field. *B–G,* selected tilted views of near native state apoA-I/HDL particles embedded in vitreous ice from six cryo-electron microscopic fields.

FIGURE 6. **Intramolecular FRET between positions 40 and 240.** Fluorescence emission (excitation wavelength 280 nm) of W@40 and W@40:L240C-AE was observed at 310–560 nm. Sample concentrations were 0.1 mg/ml. The rHDL samples W@40 and W@40:L240C-AE consisted of W@40 and AEDANS-labeled apoA-I (W@40:L240C-AE) in a 1:5 ratio with W@Ø, respectively. The W@40 and W@40:L240C-AE rHDL spectra were normalized, correcting for their proportion (1:5 with W@Ø) in rHDL. Background fluorescence was eliminated by subtracting the emission spectrum of rHDL consisting of W@Ø from the normalized emission spectrum of W@40 and W@40:L240C-AE rHDL. Energy transfer efficiency (*E*) was calculated from background corrected spectra by comparing Trp fluorescence intensities (integrated over 310–425 nm) of W@40 (donor only) and W@40:L240C-AE (donor-acceptor).

Finally, the authors used a publication recently retracted from the literature to support their model. They state, "…it is remarkable to note that the conformation of apoA-I in the (DSH) model contains several turns found in the recently reported crystal structure of lipid-free full-length apoA-I" (41).

The DSH model possesses no classic bulk bilayer lipid; rather the lipid is organized as an end-capped hexagonal I lyotropic liquid crystalline phase phospholipid. Hexagonal I phases are seen only under unique, specialized conditions; not only is this phase confined to detergents, such as lysolecithin, or perhaps to very short chained phospholipids, but it occurs only under conditions of very low water content (42).

Differential scanning calorimetry suggests that there are two distinct regions of phospholipid in nascent HDL, an annular region that cannot undergo the melting phase transition and a central bulk lipid region that has the melting phase transition of a pure bilayer of the phospholipid (43–46). Although phospholipid near the protein in the DSH model might not undergo melting, the remainder of the lipid is not remotely similar to a bilayer and is highly unlikely to undergo the melting phase transition of a pure bilayer of the phospho-

lipid. The same argument holds for high field ^{1}H NMR results that also suggest separate annular and central bulk lipid regions for nascent HDL (12, 47).

It is unclear how apoA-I could stabilize an end-capped hexagonal I lyotropic liquid crystalline phase phospholipid structure at high water concentrations in a nondetergent such as POPC. The apparent instability of such a structure is suggested by the results of our two types of MD simulations of the DSH model, all-atom and coarse-grained, in which the prolate ellipsoidal hexagonal I phase lipid particles rapidly collapse to bilayers. The fact that two entirely different types of MD simulations with different weaknesses produce the same results, DSH collapse to a discoidal bilayer structure, suggests that the starting DSH structure is unstable. The final simulated structures of the all-atom and coarse-grained apoA-I double belts are also very similar; both double belts form kinetically trapped terminal loops, further suggesting that the starting DSH structures are unstable.

Hazen and co-workers (26) recently published a 60-ns all-atom MD simulation of their original DSH model. Fig. 7 compares r.m.s.d. alignments of their simulated protein structure with our simulated 60-ns MDSA protein structure (Fig. 4*A*). The two protein conformations are remarkably similar even though the Hazen model was created by an MD simulation at 300 K (26), and our model was created by an MDSA simulation involving an initial T-jump to 500 K.

Inspection of the initial model described in Wu *et al.* (11) reveals that the central long axis of the prolate ellipsoidal hexagonal I phase lipid structure contains a linear cavity (Fig. 8*A*); this cavity has collapsed after 2 ns of MD simulation using the NPT ensemble (Fig. 8*B*). Furthermore, unlike the lipid in our final structure that is organized as a well defined bilayer (Fig. 4, *A* and *B*), the lipid in the Hazen model (26) forms a spheroidal phospholipid monolayer shell containing a large ellip-
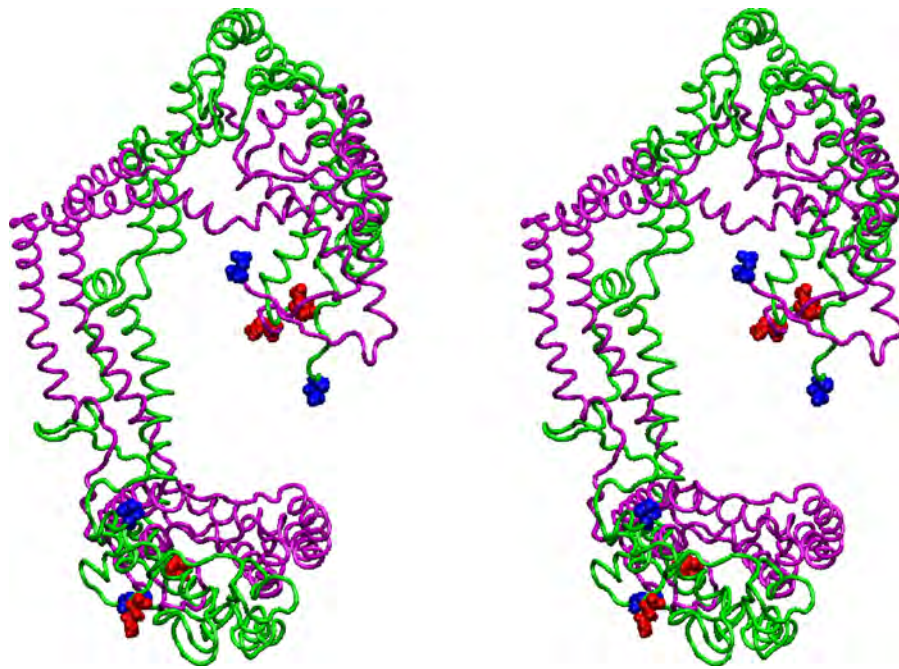
FIGURE 7. **Cross-eyed stereo image of the Cα alignment of the protein conformation of the final structure of the MD simulation by Hazen and co-workers (26) with the stereo image of our 60-ns MDSA simulation of the starting DSH model made with VMD.** The Hazen and co-workers (26) model is in *magenta,* and our 60 ns MDSA simulation of the starting DSH model (11) is in *green*. N- and C-terminal residues are space-filling *blue* and *red*, respectively.
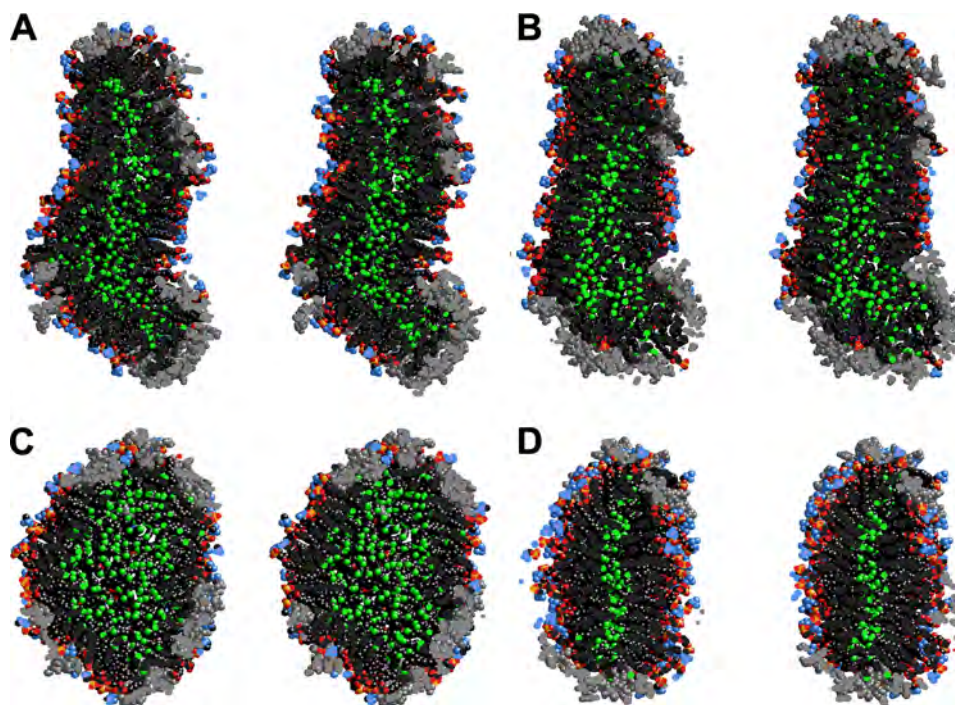
FIGURE 8. **Cross-eyed stereo images made with Rasmol showing the collapse of the central cavity in both the initial DSH model and the recently published 60-ns MD simulation of the DSH model (26) following MD simulations using the NPT ensemble.** *A,* cross-sectional image of the initial DSH model (11). *B,* cross-sectional image of the starting DSH model after a 2-ns MD simulation at 310 using the NPT ensemble. *C,* cross-sectional image of the 60-ns MD simulation of the DSH model showing the large central cavity. *D,* cross-sectional image of the 60-ns MD simulation of the DSH model after 10 ns of MD simulation at 310 using the NPT ensemble. Protein is *gray*; POPC acyl chains are *black* except for terminal methyls that are *green*; POPC head groups are *blue*, *red,* and *gold*; UC is *black*.

soidal central cavity, 30–50 Å across, that is completely devoid of matter (Fig. 8*C*).

Hazen and co-workers (26) used a canonical ensemble, *NVT* (*i.e.* the number of particles, *N*; the volume, *V*; and the absolute temperature, *T*, were kept constant) for their MD simulation. Because it corresponds most closely to laboratory conditions with a flask open to ambient temperature and pressure, the isothermal-isobaric ensemble, NPT, is more commonly used in simulations of biological molecules. For a particle surrounded by water, equilibrating the system with

Discoidal Shape of Reconstituted HDL

NPT simulations to a converged density and then switching to *NVT* would have been acceptable. However, using *NVT* without NPT equilibration produces environmental conditions that include a massive negative pressure. Such a system is not relevant for anything biological; because the volume of the periodic boundary box cannot change, it allows serious packing defects to persist during MD simulations. Because water and protein-lipid interactions inherently modulate to achieve normal bulk density, the latter due to the hydrophobic effect, this leads to a reduction in lipid density incompatible with biological systems; it is energetically much more favorable to pull interactions between lipids apart in a vacuum than interactions between either water or protein with lipid.

To confirm this for HDL, we subjected the 60-ns MD simulation of the DSH particle (26) to the same conditions that we did the starting DSH particle (11). The central cavity shown in Fig. 8*C* was emptied by deletion of water molecules placed there by VMD solvation to create empty space, followed by MD simulation under NPT conditions at 310 K. As a result, the lipid cavity began to collapse after a few nanoseconds to form an essentially complete bilayer after 10 ns of MD simulation (Fig. 8*D*). When the protein was deleted from the starting DSH particle (11), cavity collapse occurred in 5 ns (supplemental Fig. S1), indicating that the protein perhaps has a small effect on cavity stability.

Waters were removed from the central cavity because waters were stated to be missing from the Hazen structures. Our initial all-atom 5-ns 310 K simulation of Hazen's first structure was performed both with and without waters. Without water, the interior vacuum was essentially gone after 2 ns. With water, there was substantial dissipation of the interior waters after 5 ns (data not shown).

It is well known that water molecules never remain for any biologically relevant time within the hydrophobic interior of a bilayer because of the low dielectric of acyl chains; in a low dielectric, charges react with each other at long distances so that trapped water molecules move rapidly toward the bulk water. Thus, the possibility that the Hazen models contain water in their central cavities is neither physically nor biologically relevant. This result, and the fact that two entirely different types of MD simulations of the starting DSH model collapse to a discoidal bilayer structure, supports our contention that the starting DSH structure is unstable.

We used a combination of all-atom MDSA developed by trial and error to bypass kinetic energy barriers to the global structures of the particles and CGMD to achieve 18–20-μs simulations. Both methods, MDSA and CGMD, have strengths and weaknesses but not the same ones. (i) The strength of MDSA is that it is all-atom; the principal weaknesses are use of high temperature jumps and a failure to robustly sample long simulation times. (ii) The strength of CGMD is that it samples longer simulation times; the principal weakness is use of pseudoatoms to represent clusters of several atoms, more of a problem for proteins than for lipids. A second reason that we believe the DSH model is unlikely as originally published (11) is that two tomographic methods, negative stain EM and cryo-EM, unequivocally show that reconstituted apoA-I/HDL particles are discoidal in their three-dimensional shape. Discoidal structures have even been reported for large nascent HDL containing unesterified cholesterol and more than two apoA-I per disc (48).

The protocol used to examine the apoA-I/HDL particles shown in Fig. 5*A* was the same as that used to examine apoE/POPC particles in a recent publication by Ren and co-workers (29). Both NS and cryo-EM raw images and their class averages suggested that the apoE/POPC particles were spheroidal (ellipsoidal) in shape, although apoE/POPC particles were not examined by EM tomography. In contrast, both NS-EM and cryo-tomography images suggest that the apoA-I/HDL particles are discoidal.

Interestingly, the DSH model is similar to MD simulation-based models (12) in that the proposed double superhelix forms a left-handed spiral as it wraps around the central cylindrically shaped hexagonal I phase lipid micelle. The major difference in protein conformation between MD *versus* DSH models is that in the DSH model the terminal domains are separated at opposite ends of the ellipsoidal structure, although in MD models the terminal domains wrap back to self-associate (12).

Therefore, it was important that FRET spectroscopy of reconstituted apoA-I/HDL particles indicated a close intramolecular approach between residues 40 and 240 of the terminal domains, a separation of 28–34 Å that is incompatible with the mean intramolecular distance of 125 Å measured between residues 40 and 240 in the DSH model (11). Even after MD simulation of the starting DSH model, the mean intramolecular distance between residues 40 and 240 still measured 82 Å in the final MDSA model (Fig. 3*A*), 107 Å in the final CGMD model (Fig. 3*B*), and 83 Å in the 60-ns MD simulation of the DSH particle performed by Hazen and co-workers (26).

Except for the lack of self-associating terminal domains, the conformation of the surrounding apoA-I double belt in the MD-simulated DSH model (26) is similar to apoA-I conformation in our previously published MD simulations of cholesteryl ester-rich HDL particles (14). Except for its open-ended form, the DSH MD simulation (26) likely reflects conformational flexibility of the apoA-I double belt that, as the particle approaches a spheroidal shape, allows it to accommodate a cholesteryl ester-rich core through an increased twisting of a saddle-shaped apoA-I double belt structure.

Based upon these results, we suggest that, although interesting and novel, the DSH model is energetically unfavorable and not likely to be correct in its open-ended form. Rather, all of our results point to the far greater likelihood that reconstituted apoA-I/HDL particles are discoidal in shape.

REFERENCES

1. Linsel-Nitschke, P., and Tall, A. R. (2005) *Nat. Rev. Drug Discov.* **4,** 193–205

2. Forte, T., Norum, K. R., Glomset, J. A., and Nichols, A. V. (1971) *J. Clin. Invest.* **50,** 1141–1148

3. Forte, T. M., Nichols, A. V., Gong, E. L., Levy, R. I., and Lux, S. (1971) *Biochim. Biophys. Acta* **248,** 381–386

4. Sloop, C. H., Dory, L., Hamilton, R., Krause, B. R., and Roheim, P. S. (1983) *J. Lipid Res.* **24,** 1429–1440

5. Wlodawer, A., Segrest, J. P., Chung, B. H., Chiovetti, R., Jr., and Weinstein, J. N. (1979) *FEBS Lett.* **104,** 231–235

6. Atkinson, D., Small, D. M., and Shipley, G. G. (1980) *Ann. N.Y. Acad. Sci.* **348,** 284–298

7. Segrest, J. P., Li, L., Anantharamaiah, G. M., Harvey, S. C., Liadaki, K. N., and Zannis, V. (2000) *Curr. Opin. Lipidol.* **11,** 105–115

8. Martin, D. D., Budamagunta, M. S., Ryan, R. O., Voss, J. C., and Oda, M. N. (2006) *J. Biol. Chem.* **281,** 20418–20426

9. Davidson, W. S., and Thompson, T. B. (2007) *J. Biol. Chem.* **282,** 22249–22253

10. Thomas, M. J., Bhat, S., and Sorci-Thomas, M. G. (2008) *J. Lipid Res.* **49,** 1875–1883

11. Wu, Z., Gogonea, V., Lee, X., Wagner, M. A., Li, X. M., Huang, Y., Undurti, A., May, R. P., Haertlein, M., Moulin, M., Gutsche, I., Zaccai, G., Didonato, J. A., and Hazen, S. L. (2009) *J. Biol. Chem.* **284,** 36605–36619

12. Gu, F., Jones, M. K., Chen, J., Patterson, J. C., Catte, A., Jerome, W. G., Li, L., and Segrest, J. P. (2010) *J. Biol. Chem.* **285,** 4652–4665

13. Jones, M. K., Catte, A., Li, L., and Segrest, J. P. (2009) *Biochemistry* **48,** 11196–11210

14. Catte, A., Patterson, J. C., Bashtovyy, D., Jones, M. K., Gu, F., Li, L., Rampioni, A., Sengupta, D., Vuorela, T., Niemelä, P., Karttunen, M., Marrink, S. J., Vattulainen, I., and Segrest, J. P. (2008) *Biophys. J.* **94,** 2306–2319

15. Humphrey, W., Dalke, A., and Schulten, K. (1996) *J. Mol. Graph.* **14,** 33–38, 27–28

16. Kalé, L., Skeel, R., Bhandarkar, M., Brunner, R., Gursoy, A., Krawetz, N., Phillips, J., Shinozaki, A., Varadarajan, K., and Schulten, K. (1999) *J. Comp. Phys.* **151,** 283–312

17. Catte, A., Patterson, J. C., Jones, M. K., Jerome, W. G., Bashtovyy, D., Su, Z., Gu, F., Chen, J., Aliste, M. P., Harvey, S. C., Li, L., Weinstein, G., and Segrest, J. P. (2006) *Biophys. J.* **90,** 4345–4360

18. Jorgensen, W. L., Chandrasekhar, J., and Madura, J. D. (1983) *J. Chem. Phys.* **79,** 926–935

19. Brooks, B. R., Brooks, C. L., 3rd., Mackerell, A. D., Jr., Nilsson, L., Petrella, R. J., Roux, B., Won, Y., Archontis, G., Bartels, C., Boresch, S., Caflisch, A., Caves, L., Cui, Q., Dinner, A. R., Feig, M., Fischer, S., Gao, J., Hodoscek, M., Im, W., Kuczera, K., Lazaridis, T., Ma, J., Ovchinnikov, V., Paci, E., Pastor, R. W., Post, C. B., Pu, J. Z., Schaefer, M., Tidor, B., Venable, R. M., Woodcock, H. L., Wu, X., Yang, W., York, D. M., and Karplus, M. (2009) *J. Comput. Chem.* **30,** 1545–1614

20. Monticelli, L., Kandasamy, S. K., Periole, X., Larson, R. G., Tieleman, D. P., and Marrink, S. J. (2008) *J. Chem. Theory Comput.* **4,** 819–834

21. Feller, S. E., and Pastor, R. W. (1997) *Pac. Symp. Biocomput.* 142–150

22. Schlenkrich, M., Brickmann, J., MacKerell, A., Jr., and Karplus, M. (1996) in *Biological Membranes: A Molecular Perspective from Computation and Experiment* (Merz, K. M., and Roux, B., eds) pp. 31–81, Birkhauser Boston, Inc., Cambridge, MA

23. Kabsch, W., and Sander, C. (1983) *Biopolymers* **22,** 2577–2637

24. Hess, B., Kutzner, C., van der Spoel, D., and Lindahl, E. (2008) *J. Chem. Theory Comput.* **4,** 435–447

25. Marrink, S. J., Risselada, H. J., Yefimov, S., Tieleman, D. P., and de Vries, A. H. (2007) *J. Phys. Chem. B.* **111,** 7812–7824

26. Gogonea, V., Wu, Z., Lee, X., Pipich, V., Li, X. M., Ioffe, A. I., Didonato, J. A., and Hazen, S. L. (2010) *Biochemistry* **49,** 7323–7343

27. Chen, B., Ren, X., Neville, T., Jerome, W. G., Hoyt, D. W., Sparks, D., Ren, G., and Wang, J. (2009) *Protein Sci.* **18,** 921–935

28. Cavigiolio, G., Shao, B., Geier, E. G., Ren, G., Heinecke, J. W., and Oda, M. N. (2008) *Biochemistry* **47,** 4770–4779

29. Zhang, L., Song, J., Newhouse, Y., Zhang, S., Weisgraber, K. H., and Ren, G. (2010) *J. Lipid Res.* **51,** 1228–1236

30. Ren, G., Rudenko, G., Ludtke, S. J., Deisenhofer, J., Chiu, W., and Pownall, H. J. (2010) *Proc. Natl. Acad. Sci. U.S.A.* **107,** 1059–1064

31. Zheng, S. Q., Keszthelyi, B., Branlund, E., Lyle, J. M., Braunfeld, M. B., Sedat, J. W., and Agard, D. A. (2007) *J. Struct. Biol.* **157,** 138–147

32. Lagerstedt, J. O., Budamagunta, M. S., Oda, M. N., and Voss, J. C. (2007) *J. Biol. Chem.* **282,** 9143–9149

33. Cavigiolio, G., Geier, E. G., Shao, B., Heinecke, J. W., and Oda, M. N. (2010) *J. Biol. Chem.* **285,** 18847–18857

34. Nichols, A. V., Gong, E. L., Blanche, P. J., and Forte, T. M. (1983) *Biochim. Biophys. Acta* **750,** 353–364

35. Nichols, A. V., Gong, E. L., Blanche, P. J., Forte, T. M., and Shore, V. G. (1987) *J. Lipid Res.* **28,** 719–732

36. Selvin, P. R. (1995) *Methods Enzymol.* **246,** 300–334

37. Wu, Z., Wagner, M. A., Zheng, L., Parks, J. S., Shy, J. M., 3rd., Smith, J. D., Gogonea, V., and Hazen, S. L. (2007) *Nat. Struct. Mol. Biol.* **14,** 861–868

38. Shih, A. Y., Sligar, S. G., and Schulten, K. (2008) *Biophys. J.* **94,** L87–L89

39. Segrest, J. P., Jones, M. K., Klon, A. E., Sheldahl, C. J., Hellinger, M., De Loof, H., and Harvey, S. C. (1999) *J. Biol. Chem.* **274,** 31755–31758

40. Jones, M. K., Catte, A., Patterson, J. C., Gu, F., Chen, J., Li, L., and Segrest, J. P. (2009) *Biophys. J.* **96,** 354–371

41. Ajees, A. A., Anantharamaiah, G. M., Mishra, V. K., Hussain, M. M., and Murthy, H. M. (2006) *Proc. Natl. Acad. Sci. U.S.A.* **103,** 2126–2131

42. Yeagle, P. (1987) *The Membranes of Cells*, p. 68, Academic Press, New York

43. Tall, A. R., Deckelbaum, R. J., Small, D. M., and Shipley, G. G. (1977) *Biochim. Biophys. Acta* **487,** 145–153

44. Massey, J. B., Gotto, A. M., Jr., and Pownall, H. J. (1981) *Biochemistry* **20,** 1575–1584

45. Anantharamaiah, G. M., Jones, J. L., Brouillette, C. G., Schmidt, C. F., Chung, B. H., Hughes, T. A., Bhown, A. S., and Segrest, J. P. (1985) *J. Biol. Chem.* **260,** 10248–10255

46. Massey, J. B., She, H. S., Gotto, A. M., Jr., and Pownall, H. J. (1985) *Biochemistry* **24,** 7110–7116

47. Brouillette, C. G., Jones, J. L., Ng, T. C., Kercret, H., Chung, B. H., and Segrest, J. P. (1984) *Biochemistry* **23,** 359–367

48. Massey, J. B., and Pownall, H. J. (2008) *Biochim. Biophys. Acta* **1781,** 245–253